Original Research Article

GREENHOUSE GASES SCIENCE AND TECHNOLOGY

Measurements of the relative permeability to CO_2-and-brine multiphase fluid of Paaratte formation at near-reservoir conditions

Pengyu Huang, Luming Shen and Yixiang Gan, The University of Sydney, NSW, Australia
Yinjie Shen and Dongxing Du, Qingdao University of Science and Technology, Qingdao, China
Bowei Yu, Federico Maggi and Abbas El-Zein, The University of Sydney, NSW, Australia

Abstract: CO_2 sequestration in deep saline aquifers is a promising method to reduce atmospheric CO_2. The on-going CO_2CRC Otway project aims to demonstrate the effectiveness of large-scale CO_2 storage in deep saline formations and to develop new monitoring technologies in Australia. The relative permeability curves are essential for predicting the movements of CO_2 and estimate residual trapping in the aquifer during and after injection through numerical simulations. However, studies of relative permeability curves for the Paaratte sandstone at the *in situ* conditions are limited. In addition, different rock types in the Paaratte formation can behave differently when CO_2 displaces brine. This work reports four relative permeability experiments of CO_2/brine systems using the unsteady-state core flooding method for different types of rock collected from various depths of Paaratte formations at near-reservoir conditions. The relative permeability results calculated from the analytical Johnson, Bossler, and Naumann (JBN) method and the numerical history matching method are compared. The JBN method does not calculate the relative permeability accurately for CO_2/brine systems due to the assumptions of incompressible flow, since the CO_2 relative permeability results calculated from the JBN method are similar for all the cases. The history matching results show that the brine (water) relative permeability of the core samples with a high fraction of macropores is similar to the measurements for Paaratte formation reported in the literature over a large range of brine (water) saturation. In contrast, the brine relative permeability of the core samples with a high fraction of micropores is considerably higher than that of the core samples with macropores, suggesting better connectivity for the samples with a high fraction of micropores. The new findings will be useful in reservoir-scale numerical modelings of the Paaratte formation to more accurately predict the movement of CO_2 during and after the injection.

Additional supporting information may be found online in the Supporting Information section at the end of the article.

Keywords: carbon storage; CO_2-brine multiphase fluids; CO_2 drainage; core flooding experiments; relative permeability

Correspondence to: Luming Shen, School of Civil Engineering, The University of Sydney, Sydney, NSW 2006, Australia.
E-mail: luming.shen@sydney.edu.au
Received September 12, 2020; revised March 6, 2021; accepted April 13, 2021
Published online at Wiley Online Library (wileyonlinelibrary.com). DOI: 10.1002/ghg.2074

Introduction

Carbon capture and storage in depleted reservoirs and deep saline aquifers play an important role in reducing CO_2 atmospheric concentration, a leading cause of global warming.[1] The long-running CO_2CRC (The cooperative research center for greenhouse gas technologies) Otway project has been demonstrating the feasibility of CO_2 storage in depleted gas reservoir and deep saline formations in the Otway Basin, in Victoria, Australia, through Stage 1 and Stage 2, respectively.[2] The injected and stored CO_2 in the saline formation requires long-term monitoring. Hence, in Stage 3, the project aims to develop a cost-effective subsurface monitoring system by reducing the surface footprint.[3] An injector CRC-3 well was drilled and will be used for a small injection of CO_2 ($<$ 30 000 tones) for the project.[4] A comprehensive site characterization in the Otway basin is essential in evaluating the injection performance, and understanding the migration of the CO_2 plumes after injection using numerical tools. Due to the heterogeneity of the saline reservoir, site characterizations are challenging. Recently, Mishra *et al.* (2019) carried out a high-resolution rock characterization for the two parasequences from the lowermost units of Paaratte formation using rock properties such as porosity, permeability, capillary entry pressure, mineral composition, and grain size distribution obtained through discrete cores and log data from the wells in the Otway basin.[5] The results of the characterization can be used to run detailed flow simulations. However, the relative permeability for various types of rock, which is essential in modeling the multiphase flow for reservoirs, was not measured in their studies. To improve our understanding of multiphase flow and CO_2 trapping in saline aquifers, the relative permeabilities to CO_2/brine systems from the core flooding experiment at different depths or for different types of rocks from Paaratte formation are needed. The relative permeability curves to CO_2/brine fluids used in flow transport modeling has a significant effect on predicting the footprint of CO_2 plumes, pressure variations, and overall CO_2 storage in a reservoir.[6–9]

Measurements of relative permeability to CO_2/brine systems were only carried out from the earlier 2000s. Bachu and Bennion reported the relative permeability measurements to CO_2/brine systems at in-situ conditions for sandstone, carbonate, shale, and Anhydrite rocks.[10] For the drainage process, a low endpoint value was observed: the average CO_2 relative permeability at maximum CO_2 saturation was 0.269, and the average maximum CO_2 saturation was 50%.[10] Later, Bachu reported 16 more relative permeability test results for sandstone rocks,[11] showing that there was no correlation between porosity and pore size distribution, and no clear correlation could be found between relative permeability characteristics and petrophysical rock properties, although the irreducible brine saturation broadly increased with the absolute permeability. It should be noted that in-situ pressure, temperature, and salinity were used for each test on the rock sample in the setup reported by Bachu and Bennion[10] and Bachu,[11] which means these conditions were different for each test, and it is difficult to separate their effects on relative permeability. Apart from the work of Bennion and Bachu[10] and Bachu,[11] most measurements were done for Berea and a few other types of sandstone.[12–14]

While the two-phase flow depends on the morphology of the rock at pore scales, it also depends on viscosity ratio, and capillary number, which is the dimensionless measure of the ratio of viscous force to interfacial force across the interface between two fluids.[15] Therefore, the interfacial tension and viscosity ratio have an impact on the relative permeability. Pini and Benson studied experimentally the capillary pressure and relative permeability curves of Berea sandstone using different fluid pairs (gas CO_2/water, gas N_2/water, and supercritical CO_2/brine), which represented cases with different interfacial tension (achieved with different pressures) and kept a similar viscosity ratio between the fluid pairs.[12] Their results showed that the capillary pressure was affected by the interfacial tension consistently, that is, the capillary entry pressure used in the Brooks–Corey equation increased with the increase of interfacial tension. The relative permeability curves obtained from the drainage process were similar at different interfacial tensions, suggesting no significant effects of the interfacial tension on the relative permeability curves. However, an earlier experimental work of Bachu and Bennion suggested that the interfacial tension can have an impact on the relative permeability curve. Specifically, the endpoint values of the CO_2 relative permeability decreased with the increase of interfacial tension, and the irreducible water saturation increased with the increase of interfacial tension (for drainage).[16] Still, the viscosity also varied along with varying interfacial

  | *Greenhouse Gas Sci Technol*. **11**:697–711 (2021); DOI: 10.1002/ghg.2074

tension in their studies.[16] Jeong *et al.*[14] found that the CO_2 and brine relative permeability increases with the increase in viscosity ratio (viscosity of CO_2 to viscosity of water), and the residual brine saturation increased (relative permeability curves moved from low to high brine saturation) with increases in interfacial tension. Their findings on the effect of interfacial tension supported those of Bachu and Bennion.[16] For the effect of interfacial tension, they suggested that the adhesive force between immiscible fluids and porous media was larger with greater interfacial tension. Hence, water was more difficult to flow out during drainage, which results in more residual brine saturation in the rock. An increase in CO_2/brine viscosity ratio may lead to CO_2 flowing through the large pore neck (for water-wet sandstones) and hence an increase in CO_2 relative permeability.[14] The increase of brine relative permeability was attributed to lower viscosity of the brine used in the test by Jeong et al.,[14] with water flowing more easily. Since the pressure and temperature have a direct impact on the fluid properties, such as density, viscosity, and interfacial tension, the relative permeability results can hence be affected as well. For example, Liu *et al.* obtained the permeability curve for the CO_2/brine system on Berea sandstone by varying pressure from 8.27 to 17.9 MPa and temperature from 19 to 38°C.[17] Their results showed that pressure had a strong effect on relative permeability, as the endpoint relative permeability increased from 32.4 to 46.8%.[17] Therefore, to reflect the CO_2/brine flow in real reservoir conditions, it is important to perform the core flooding experiments at the *in situ* pressure and temperature conditions for the studies of natural reservoirs.

For the relative permeability measurement in Paaratte formation, Krevor *et al.* reported the relative permeability and residual trapping data for the CO_2 and brine in a Paaratte sandstone collected at 1400 m, and at a temperature of 50°C, a fluid pressure of 9 MPa, and a confining pressure of 11.7 MPa.[13] Although the studied Paaratte sandstone has several low porosity beddings perpendicular to the flowing direction, the relative Paaratte sandstone showed general similarity with the homogenous Berea sandstone in their studies,[13] and therefore, they suggested that the bulk rock properties dominate local heterogeneities in this case. As mentioned above, the controls on temperature and pressure can affect the dynamics in the core flooding. Temperature, fluid pressure, and confining pressure in Krevor *et al.*[13] are smaller than those prevalent at reservoir conditions, that is, $T = \sim 60$°C,[18] and $P = \sim$13–14 MPa (estimated from the pressure gradient of 9.56 MPa km^{-1} in Otway Basin[19]), and the confining pressure $P_{conf} = \sim 32$ MPa (estimated from the average vertical stress gradient of 21.45 MPa/km[20]). Later, Reynolds[21] also reported the site-specific relative permeability for a homogenous Paaratte sandstone collected at a depth of 1498.5–1498.8 m from the CRC-2 well with relevant temperature and fluid pressure for the sites ($T = 63$°C and $P = 12.5$ MPa) with both drainage and imbibition tests conducted in her PhD thesis.[21] The confining pressure in the test was reported to be 3–5 MPa above the pore pressure, which was also smaller than the *in situ* confining pressure. It is possible that the effective stress can have an impact on the relative permeability results as well, according to experimental studies on oil/water relative permeability.[22] Hence, it is better to use the *in situ* confining pressure for the measurement of the CO_2/brine relative permeability for the Paaratte formation.

It was found that only a few tests were reported for the Paaratte sandstone in the literature, and these tests are for the cores with high absolute permeability (i.e., permeability > 1 Darcy).[13,21] Although the Paaratte formation is generally considered to have high absolute permeability, different Paaratte formation facies at different depths can have different permeabilities ranging from 0.01 millidarcy (mD) up to serval Darcy (D).[5,23] Since the relative permeability was highly site-specific and depended on the rock types,[11] the study of the relative permeability of CO_2/brine flow for different types of rocks can potentially help to develop a detailed reservoir model for monitoring the CO_2 plume during and after injection. In this work, we aim to measure, for the first time, the relative permeability of three sandstones with different absolute permeability, obtained at various depths from the lowermost unit of Paaratte formation with core flooding experiments under realistic reservoir conditions. The relative permeability curves are calculated using the Johnson, Bossler, and Naumann (JBN) methods[24] and the history matching method in this work. Mercury intrusion capillary tests are also performed to obtain the pore size distribution and the capillary pressure curves, which can be used to characterize the pore structures for different rocks. The results will help in improving our understanding of

Table 1. The properties of raw sample cores from CRC-3 well.

Raw sample No.	Tray No.	Start depth (m)	End depth (m)	Rock type	Diameter (mm)	Length (mm)	Depositional facies
1	CRC3-Tray 14	~1470.92	~1471.02	Cross-bedded fine-grained sandstone	68	100	Distal mouthbar
2	CRC3-Tray 19	~1487.00	~1487.10	Laminated sandstone	69	80	Proximal mouthbar
3	CRC3-Tray 22	~1495.27	~1495.38	Massive fine-grained sandstone	70	105	Proximal mouthbar

multiphase flow in different rock types for the Paaratte formation.

Experimental methods

Rock samples

The rock samples were collected from the CRC-3 well at various depths of the lowest unit of the Paaratte formation from the Otway project. Details of the rock samples are given in Table 1. The rock samples were cored into cylinders for core flooding tests with a diameter of 25 mm and a length of ~38–68 mm. The locations, dimensions, and porosity of the samples are listed in Table 2, where the number in the core sample name refers to the raw sample number in Table 1, and the letter indicates the coring direction, that is, V for vertical, and H for horizontal. The porosity of the core samples was obtained by using an automatic porosity and permeability measurement apparatus (Model TCKS-400). There are five facies as follows: delta front, distal mouthbar, proximal mouthbar, distributary channel, and carbonated-cemented sandstone, for the lowest unit of the Paaratte formation.[4,5] Based on the depositional facies log for CRC-3 well,[5] sample 1 belongs to the distal mouthbar, and samples 2 and 3 are proximal mouthbar (Table 1). The distal mouthbar is a mud-rich section, which consists of fine-interbedded silts and fine-grained sandstones, while the proximal mouthbar is mainly the moderately-sorted to well-sorted, fine-grained sandstones.[4]

Measurement of capillary pressure curves

The capillary pressure–saturation curves were measured by conducting the mercury injection capillary pressure (MICP) tests using a Micrometritics Autopore IV. The capillary pressure value can be converted from Hg/vacuum pair fluids to CO_2/brine pair using the following equation[25]:

$$P_{c,\mathrm{cb}} = \frac{\gamma_{\mathrm{cb}} \cos\theta_{\mathrm{cb}}}{\gamma_{\mathrm{hv}} \cos\theta_{\mathrm{hv}}} P_{c,\mathrm{hv}} \quad (1)$$

where P_c is the capillary pressure; γ is the interfacial tension, and θ is the contact angle. The subscripts hv and cb refer to the Hg/vacuum system and the CO_2/brine system, respectively. Here, the contact angle for the CO_2/brine (or water) system is assumed to be the same as the value in the mercury/vacuum system, as suggested in Krevor *et al.*[13]. For the values of interfacial tension, $\gamma_{\mathrm{cb}} = 30.5$ mN m^{-1} (at $T = 60$°C and $P = 14$ MPa) and $\gamma_{\mathrm{hv}} = 485$ mN m^{-1} were used. The interfacial tension of CO_2/brine here was obtained from the interfacial tension of CO_2/water at relevant temperature and pressure,[26] since a low salinity brine (800 ppm) was used in this work.

Table 2. The dimensions of the core samples and the injection rate used for core flooding test.

Core sample name	Diameter (mm)	Length (mm)	Injection rate at drainage (mL min^{-1})
1V	25	67.5	1
1H	25	44.5	5
2V	24.5	38.2	10
2H	25	47.2	-*
3V	24.2	66	10

*Core 2H was not tested for relative permeability.

Core flooding test

The absolute permeability was measured for all cores, while the Cores 1V, 1H, 2V, and 3V were subjected to

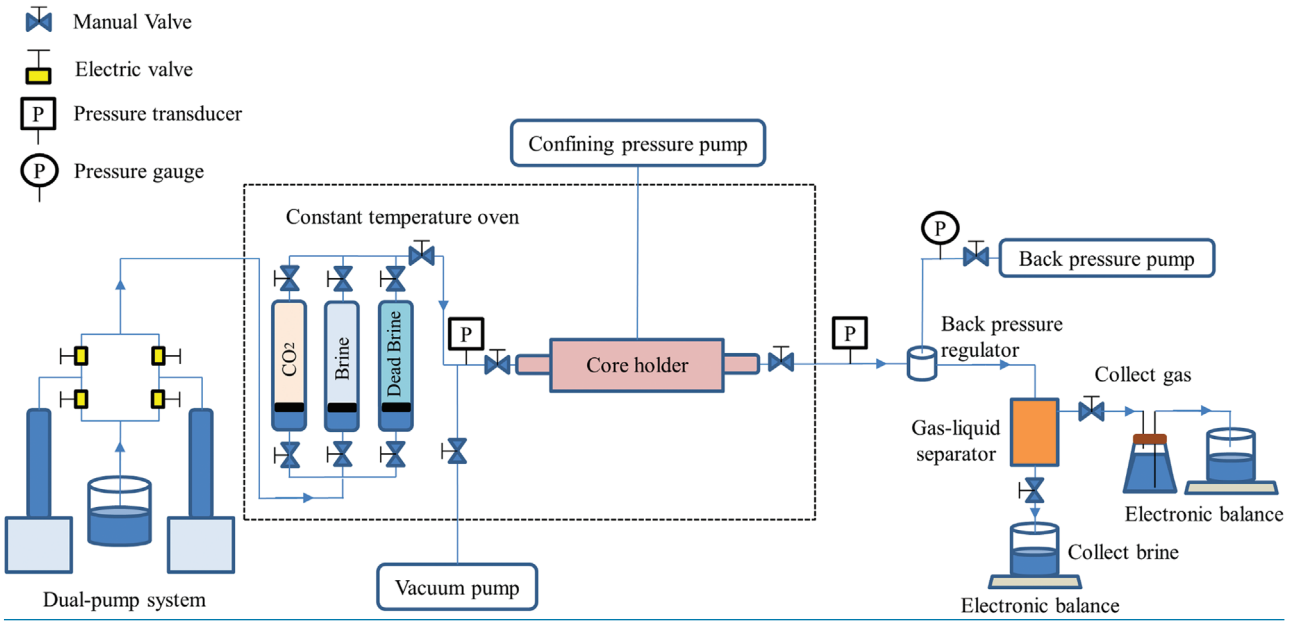

Figure 1. A schematic diagram of the core flooding experiment setup.

the relative permeability measurement. A schematic diagram of the setup of the core flooding experiment is given in Fig. 1, which is based on the multifunctional core flooding facility for high-pressure and high-temperature conditions (Model TC-2). The setup can maintain a temperature between 25 and 150°C and pressure from 0 to 70 MPa. Three types of fluids were used in the core flooding experiments: CO_2-saturated brine, brine-saturated CO_2, and dead brine (brine with no dissolved CO_2). A brine salinity of 800 ppm (NaCl) was used since such salinity was found in the formation.[18,27] The dual-pump injection system, combined with fluid bottles, provided a continuous injection of the fluid into the core holder. The temperatures of the injected fluids and the core holder were controlled in the oven, as shown in Fig. 1. Pressure transducers were used to record the pressure of the fluids at the inlet and outlet of the core holder, and the data were collected by a computer in real-time. The confining pressure of the core sample was automatically controlled with a pump. A back-pressure regulator, along with a hydraulic pump, was used to control back pressure at the outlet. The fluids eventually passed through a two-phase (gas–liquid) separator, and CO_2 then flowed into a sealed flask with a stopper and a tube to a beaker. The beaker was placed on top of an electronic scale (with a measurement uncertainty of 0.0001 g). However, since the pressure was not controlled in the two-phase separator and the mass of CO_2-induced water reached the upper limit of the electronic scale quickly, this setup could only be used to measure the CO_2 break-through time, that is, up to when CO_2 started to flow out during the drainage process. The brine from the two-phase separator was collected and its weight measured as a function of time, using an electronic balance (with a measurement uncertainty of 0.001 g), which was connected to a computer for data logging.

The core samples were dried at 100°C for at least overnight before the core flooding test. A dried core sample was wrapped with aluminum foil and heat-shrinkable Teflon and then placed in a Viton rubber sleeve. The aluminum foil was used to prevent the corrosion of the rubber sleeve from CO_2. After placing the core sample inside the core holder, the vacuum was performed overnight to extract the air out of the core sample. For the core flooding test, the temperature was kept at 60°C based on the thermal profile of the CRC-2 well, which was assumed to be similar to the thermal profile of the CRC-3 well.[18] The confining pressure was calculated from the average vertical stress gradient (21.45 MPa km^{-1}) at the Otway Basin, as measured in Vidal-Gilbert et al.[20] since the rock samples were obtained at a depth between 1470 m and 1500 m. The average pore pressure gradient was estimated to be 9.56 MPa km^{-1} from the well data at the Otway Basin,[19] and hence, pore pressures could be calculated accordingly. Therefore, an average confining

pressure P_{conf} of 32 MPa and an average back pressure P_{back} of 14.2 MPa were used for all cases.

Once the vacuum process was completed, the injection of dead brine started. The temperature T was set at 60°C during the injection. P_{conf} and P_{back} were increased gradually to the experimental values, that is, $P_{conf} = 32$ MPa and $P_{back} = 14.2$ MPa, during the brine injection. At least five pore volumes of the dead brine were injected to saturate the core at the targeted temperature and pressure. At this stage, the absolute brine permeability was measured accordingly. Afterward, at least five pore volumes of the CO_2-saturated brine were injected to the core at a constant rate to saturate the core and prepare for the drainage test.

Next, the brine-saturated CO_2 was injected into the core at a constant rate. The injection rate was also listed in Table 2. Different injection rates were applied to ensure a relatively large pressure drop and a low capillary number $Ca = v\mu/\gamma < 10^6$, where v is the Darcy's velocity, μ is the viscosity of the fluid, and γ is the interfacial tension. The volume of effluent brine and the differential pressure were recorded in real-time. The injection of brine-saturated CO_2 was completed when there was no more effluent brine. At the end of the experiment, the weight of the core sample was measured to verify the endpoint saturation for the drainage test. The JBN methods[24] were used to calculate the relative permeability to brine and CO_2, that is, k_{rb} and k_{rco_2} at the outlet face of the core, as:

$$k_{rb}\left(S_{co_2,\,o}\right) = \frac{f_b}{d\left(\frac{1}{W_{in}I_R}\right)/d\left(1/W_{in}\right)}, \tag{2}$$

$$k_{rco_2}\left(S_{co_2,o}\right) = \frac{f_{co_2}\mu_{co_2}k_{r,\,b}}{f_b\mu_b} = \frac{\left(1-f_b\right)\mu_{co_2}k_{r,\,b}}{f_b\mu_b}, \tag{3}$$

where W_{in} is the cumulative volume of injected CO_2 divided by pore volume; μ_b and μ_{co_2} are the viscosity of brine and CO_2, respectively; f_b and f_{co_2} are the fractional flow of brine and CO_2 at the outlet face of the core, respectively; I_R is the relative injectivity; $S_{co_2,o}$ is the CO_2 saturation at the outlet face of the core. f_b, I_R, and $S_{co_2,o}$ can be calculated from the following equations:

$$f_b = \frac{dS_{co_2,\,ave}}{dW_{in}} = \frac{dW_{b,\,out}}{dW_{in}}, \tag{4}$$

$$I_R = \frac{q_{in}/\Delta P}{\left(q_{in}/\Delta P\right)_i}, \tag{5}$$

$$S_{co_2,o} = S_{co_2,\,ave} - W_{in}f_b, \tag{6}$$

where $S_{co_2,ave}$ is the average CO_2 saturation in the core; $W_{b,out}$ is the cumulative volume of the produced brine in pore volume; q_{in} is the flow rate of the injection; ΔP is the pressure drop across the core sample; $(q_{in}/\Delta P)_i$ indicates the value of $(q_{in}/\Delta P)$ at the start of injection. The brine saturation S_b can be calculated $S_b = 1 - S_{co_2,o}$. The viscosity of brine at high pressure and temperature was assumed to be the same as that of water, and the viscosity of water and CO_2 were obtained from Lemmon et al.[28] The weight of the produced brine was converted to the cumulative volume of the produced brine $W_{b,out}$. The reading of the balance for the produced brine was recorded in real-time. Hence, the recorded mass of brine was not always balanced out, and sometimes a greater mass was observed due to the impact force from the effluent brine, with the reading subsequently dropping to a balanced value. Those unbalanced readings were considered as the outliers and removed manually from the data, which allows more accurate differentiation of the raw data in Eqn (4). A linear function was used to fit $(1/W_{in}I_R)$ as a function of $(1/W_{in})$, and a constant slope was used in the calculation of Eqn (2). The void volume in the tube and pressure transducers, which could store excess brine, was taken into account. In the core flooding experiment, the brine in tubes at the upstream (before the inlet face of the core) could be removed using the vacuum pump when turning off the valves at the inlet face of the core and near the fluid bottles before injecting CO_2. The brine volume in the downstream tube and pressure transducer could not be vacuumed due to the limitations of the setup. The void volume of the downstream tubes and pressure transducer was estimated by pumping air into the tube filled with water, which is ~7.5 mL. Since we observed that the CO_2 flowed out at a time when most of the brine had been displaced, it was assumed that the initially produced brine volume of ~7.5 mL was not included in the calculation.

The JBN method has been developed for homogenous rock and incompressible fluids, and it does not consider capillary-end effects. Hence, the history matching method is also applied and compared with the JBN method. The history matching method is a numerical procedure for simulating a

one-dimensional core flooding test, under given physical properties of the rock (e.g., dimensions, porosity, and absolute permeability), as well as the relative permeability and capillary pressure curves. It is possible to adjust parameters of relative permeability models to back fit numerical predictions to historical records of brine production and pressure drop data during the experiments, hence generating estimates of the relative permeability of the cores. The MATLAB Reservoir Simulator Toolbox (MRST), which is an open-source reservoir modeling code, was used for modeling the core flooding test.[29] It has been shown in Manasipov and Jenei[30] that MRST is capable of reproducing the core flooding results from the well-known simulators, for example, Sendra, CYDAR, PORLAB, and Scores. The capillary pressure curve obtained from the MICP test is also an input of the 1D core flooding model based on a fitted exponential function. The relative permeability curves are described by the Corey functions:[31]

$$k_{rb} = (S_{\text{eff}})^{N_b}, \tag{7}$$

$$k_{r\text{co}_2} = k_{r\text{co}_2}\ (S_{bi})\,(1 - S_{\text{eff}})^{N_{\text{co}_2}}, \tag{8}$$

$$S_{\text{eff}} = \frac{S_b - S_{bi}}{1 - S_{bi}}, \tag{9}$$

where S_b is the brine saturation, and S_{eff} is the effective brine saturation; S_{bi} is the irreducible brine saturation; k_{rco2} (S_{bi}) is the relative permeability at S_{bi}; k_{rco2} (S_{bi}), $N_{b,}$ and N_{co_2} are the adjusted parameters in the history matching method. The optimization can be done manually or automatically. In this study, the optimization is done through MATLAB nonlinear optimization algorithm, by finding the minimum of the objective function g:

$$g = \frac{1}{2}\sum_{i}^{N}\left(\left(\frac{\Delta P_{\text{i}}^{\text{sim}} - \Delta P_{\text{i}}^{exp}}{\Delta P_{\text{i}}^{exp}}\right)^2 + \left(\frac{Q_{\text{bp, i}}^{\text{sim}} - Q_{\text{bp, i}}^{\text{exp}}}{Q_{\text{bp, i}}^{\text{exp}}}\right)^2\right), \tag{10}$$

where $\Delta P_{\text{i}}^{\text{sim}}$ and $\Delta P_{\text{i}}^{\text{exp}}$ are the simulation and experimental pressure drop across the core at different times, respectively; $Q_{\text{bp, i}}^{\text{sim}}$ and $Q_{\text{bp, i}}^{\text{exp}}$ are the simulation and experimental brine production at different times, respectively; N is the number of experimental data points that are used in history matching.

Results and discussion

The average and median pore diameters measured in the MICP tests are reported in Table 3. The median pore diameter is calculated as the pore diameter at 50% of the intruded mercury volume. It can be seen from Table 3 that this varies from ~2 to ~ 46 μm for the three tested samples. The median pore diameter of sample 1 is close to the average pore diameter, while those of samples 2 and 3 are much larger than their averages. In general, both average and median pore diameters increase from sample 1 to 3, and sample 1 has the smallest average and median pore diameters among the three samples. The log differential intrusion volume plots, that is, $dV_n/d\log(D)$ against D, are also shown in Fig. 2(a) for the three samples, where V_n is the normalized intrusion volume, and D is the diameter of the pore. The $dV_n/d\log(D)$ is used for the pore size distributions of the tested samples as the diameter of the pore is plotted at the logarithm scale, although it emphasizes the macropores region.[32,33] Samples 1 and 2 have micropores (less than 1 μm), as shown in Fig. 2(a). Besides, sample 2 has a smaller pore size than sample 1, but it also has a larger spread than sample 1. Hence, sample 2 covers a broad range of pore sizes from 0.05 to 350 μm (Fig. 2(a)). A peak is observed at the large pore region (21 μm) for sample 2. Sample 3 has the largest pores among the three samples, and most pores of sample 3 have a diameter between 2 and 350 μm. The capillary pressure against the vacuum saturation, that is, 1 – S_{Hg}, where S_{Hg} is the mercury saturation calculated by the ratio of injected mercury at each pressure to the total injected mercury, as shown in Fig. 2(b). It is assumed that mercury can access all of the pores of the tested rock sample, and hence the zero vacuum saturation is observed at the end. The capillary pressure presented here is converted for the CO_2/brine system using Eqn (1). In general, the sample with a larger average and median pore diameters has a lower capillary pressure at a specific saturation value.

The porosity and absolute brine permeability of the core samples are reported in Table 3. The absolute permeability varies widely for the tested samples, even if all samples are identified as sandstones with a relatively large porosity (above ~ 25%). For example, Core 1V has the smallest permeability (0.11 mD), and Core 3V has the largest permeability (330 mD). In general, the pore diameter and the pore size distribution have a significant effect on the absolute permeability,[34] which is also observed from our results.

Table 3. The average and median pore sizes of the tested samples measured by MICP and the absolute brine permeability and porosity of the core samples.

Sample No.	Average pore diameter (μm)	Median pore diameter (μm)	Core sample name	Brine permeability (mD)	Porosity (%)
1	1.93	5.5	1V	0.11	26
			1H	0.55	24.8
2	3.51	25.3	2V	3.34	29.1
			2H	292	29.6
3	45.8	137.4	3V	330	34.6

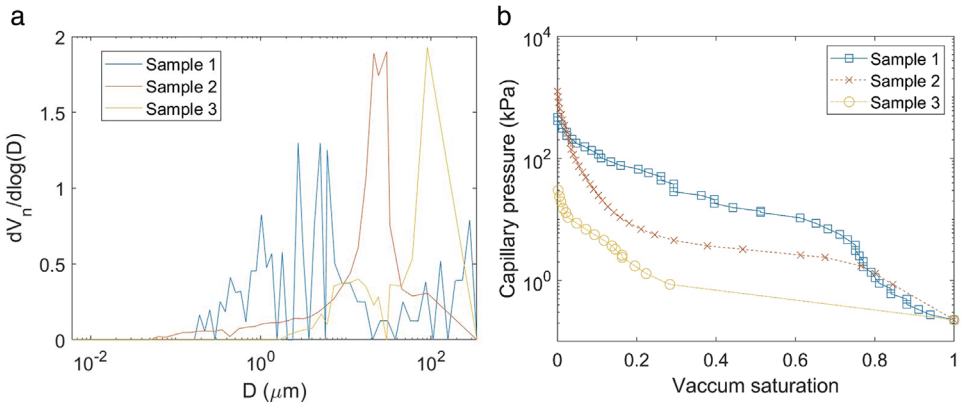

Figure 2. (a) The log differential intrusion volume (normalized) against the diameter of the pore at the logarithm scale; (b) capillary pressure (at the logarithm scale) against vacuum saturation obtained from MICP test and converted for CO_2/Brine systems using Eqn (1). The pore size distribution and capillary pressure data are reported in Sections S1 and S2 in Supporting Information.

If we only consider the vertical cores, there is a positive correlation between the pore diameter and absolute permeability (Fig. 3). The permeability of samples in different directions can vary. While the absolute permeability of Core 1H is five times that of Core 1V, the absolute permeability of Core 2H is two orders of magnitude greater than that of Core 2V. The large difference in absolute permeability between Cores 2V and 2H may be attributed to the fact that they are laminated sandstones with multiple bedding layers in the vertical direction (Table 1). Overall, the vertical permeability is smaller than the horizontal one, which is consistent with the literature.[35]

The relative permeability results from the JBN method and the history matching method are compared in a semilog plot (Fig. 4). The final parameters of the relative permeability model calculated from the history matching method are given

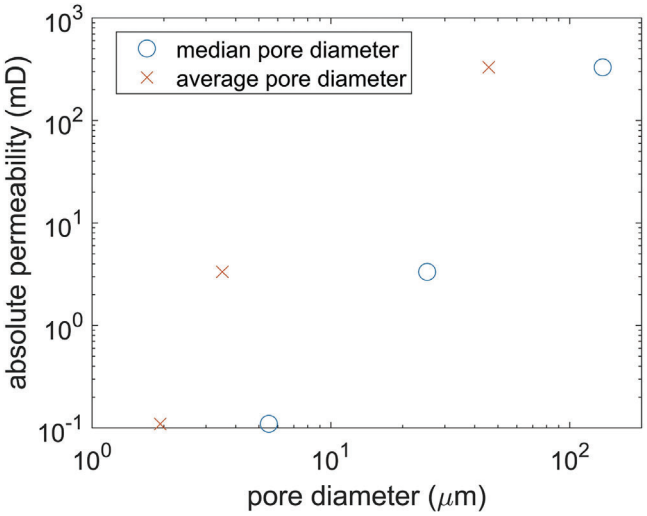

Figure 3. The absolute permeability against the average and median pore diameters.

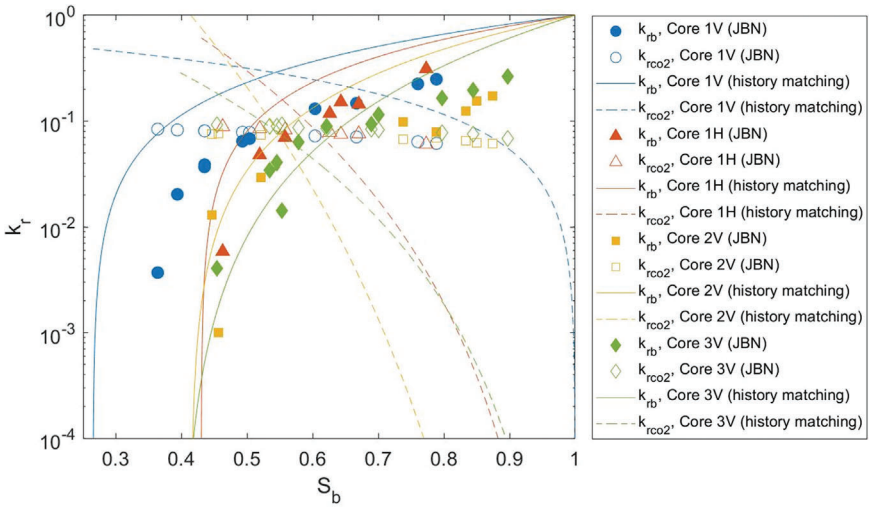

Figure 4. The relative permeability curves at different brine saturation (S_b) for Cores: 1V, 1H, 2V, and 3V, obtained from both JBN and history matching methods. The JBN relative permeability data in this work are reported in Section S3 in Supporting Information.

Table 4. The final parameters of the Corey functions for relative permeability curves calculated from the history matching method.

Core sample name	Irreducible brine saturation S_{bi}	$k_{rco2}(S_{bi})$	N_{co_2}	N_b
1V	0.265	0.4836	1.1	1.279
1H	0.430	0.6144	5.525	1.201
2V	0.414	0.9986	9.879	1.757
3V	0.398	0.2875	4.580	2.713

in Table 4. The brine relative permeability curves calculated from the history matching method are generally greater than those calculated from the JBN method, although the brine relative permeability results of Core 3V calculated from both methods are quite similar for $S_b < \sim 0.7$. The CO_2 endpoint permeability values calculated from the history matching method are greater than those calculated from the JBN method. The difference in the relative permeability curves between the two methods is probably caused by the fact that the effects of compressibility of the CO_2 phase are not considered in the JBN method. Although CO_2 is at its supercritical state in the experiments considered here, it is still compressible, and its viscosity can change at different fluid pressures. All in all, it seems that the JBN method is not able to capture the CO_2 relative permeability curves accurately since all the curves are relatively flat and quite similar for the different cores. The CO_2 relatively permeability curves from the history matching method appear to better describe the multiphase flow behavior in the tested cores. The Core 3V has the smallest CO_2 endpoint relative permeability among the tested cores. If one focuses on the results of the history matching method, Core 1V has the highest brine relative permeability curves, followed by Core 2H, Core 2V, and then Core 3V. A similar trend can be observed from the JBN results as well except that the brine relative permeability of Core 3V is higher than that of Core 2V. The difference in relative permeability curves between Core 1V and 1H can be due to the subcore heterogeneity and lamination of the rock.[36] The brine relative permeability of both Cores 1V and 1H are generally greater than those of Cores 2V and 3V, which can be observed from both the JBN and history matching method. The results suggest that the relative permeability of rocks with a higher proportion of micropores is higher than those with more macropores, which means the Cores 1V and 1H can have better brine and CO_2 connectivity than Cores 2V and 3V. Water can possibly flow through corners of the pores in the water-wet rock, which is known as the corner flow phenomenon.[37] Hence, if the Cores 1V and 1H have more small pores and better grain connectivity than Cores 2V and 3V, the corner flow could be why they have a greater brine relative permeability. Although Core 2V (sample 2) has low absolute

Table 5. The absolute permeabilities, irreducible brine saturation, and fitted parameters of the core samples for the results from the JBN method.

Core sample name	Brine permeability (mD)	Irreducible brine saturation S_{bi}	$k_{rco2}(S_{bi})'$	N_{co_2}'	N_b'	95% Confidence bounds of N_b	R^2 for k_{rb}
1V	0.11	0.265	0.145	30.5	3.5	[2.96, 4.07]	0.76
1H	0.55	0.430	0.135	21.9	2.11	[1.9, 2.32]	0.94
2V	3.34	0.414	0.106	38.4	6.39	[5.38, 7.4]	0.70
3V	330	0.398	0.166	47.0	5.57	[4.13, 7.02]	0.39

permeability and a small number of micropores, it has a broad spread of pore size distribution and contains macropores. The majority of pores in sample 1 are in the range between 0.2 and 20 μm, and most of them are micropores (Fig. 2(a)). It should be recalled that sample 1 belongs to the distal mouthbar facies, and samples 2 and 3 are from proximal mouthbar facies. The results suggest that there is a clear difference in the relative permeability curves between distal mouthbar and proximal mouthbar facies.

For further comparison of the results between the JBN method and the history matching method, the results of the JBN methods are fitted with the Brooks–Corey equations:[13,31]

$$k_{rb,\,bc} = (S_{\text{eff}})^{N_b'}, \tag{11}$$

$$k_{rco_2,\,bc} = k'_{rco_2}\,(S_{bi})\,(1 - S_{\text{eff}})^2(1 - (S_{\text{eff}})^{N'_{co_2}}), \tag{12}$$

where S_b and S_{eff} are the brine saturation and effective brine saturation (see Eqn (9)), respectively; $k_{rco2}'(S_{bi})$ is the relative permeability at irreducible brine saturation S_{bi}; N_b' and N_{co_2}' are fitting parameters. It should be noted that the irreducible saturation can be related to the achievable capillary pressure in the experiments. Here we assume that the endpoint saturation obtained from the experiments is the irreducible brine saturation. Hence, $k_{rco2}'(S_{bi})$ is considered as a fitting parameter as well, unlike in Krevor *et al.*[13] where it was assumed to be 0.95, and the values of the fitting parameters are reported in Table 5. The fitting curves are plotted as the dashed lines in Fig. 5 and compared with the curves obtained from the history matching method (solid lines). It should be noted that the Brooks–Corey equations do not fit well for the brine relative permeability curve of Core 3V, with a low R^2 value of 0.39. The R^2 values for fitting the Brooks–Corey equation to the CO_2 relative permeability are negative, suggesting that the Brooks–Corey equation (Eqn (12)) does not provide a good description of the experimental CO_2 relative permeability. Hence, the fitted values $k_{rco_2}'(S_{bi})$ and N_{co_2}' are not meaningful here. This may be due to the calculation errors in the JBN method. The fitted parameter for brine relative permeability (N_b') is more relevant, and the 95% confidence interval of N_b' is provided in Table 5. All the cases have a brine saturation around 0.4, except for Core 1V, which has an irreducible brine saturation of 0.265. It should be noted that the fitted equation of brine relative permeability (Eqn (11)) is the same as the brine relative permeability model used in the history matching method (Eqn (7)). Although the curves are different, both fitted parameters N_b' (see Table 5) and the final history matching parameters N_b (see Table 4) tend to increase with the increase of the pore size of the core samples. The results indicate that the JBN method can also capture the changes in the flow behavior of brine due to the variations of the microstructures to a large extent. However, the JBN method cannot obtain the relative permeability curves accurately. From the results of the history matching method, there is no correlation between the average pore size and the endpoint relative permeability, nor between the average pore size and endpoint saturation. The endpoint saturation can be related to the heterogeneity of the rock or the achievable capillary pressure during the experiments.[13,38] Core 3V has a relatively low endpoint permeability. The low endpoint relative permeability can be limited due to the experimental conditions, and it may also be challenging to achieve the real irreducible brine saturations in reservoir conditions.[21,39]

Krevor *et al.* carried out a steady-state core flooding test for CO_2/water systems at 50 °C and a pore pressure

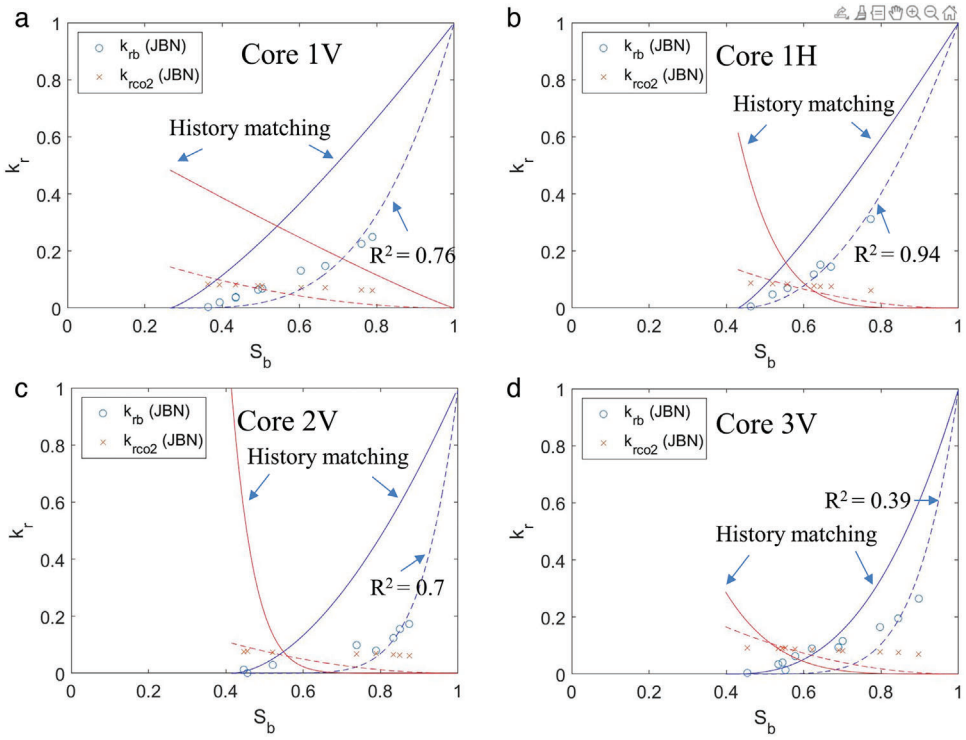

Figure 5. The relative permeability curves with the fitted curves (dash line) at different brine saturation (S_b) for the results calculated from the JBN method and compared with the results of the history matching method (solid lines).

of 9 MPa with X-ray computed tomography techniques for four types of rocks.[13] One of the rocks was obtained at a depth of 1400 m from Paaratte sandstone formation,[13] which is at a similar depth for the cores we tested in this work. Reynolds[21] also applied a similar experimental design as reported in Krevor *et al.*[13] to measure the relative permeability of a homogenous Paaratte sandstone core obtained from CRC-2 well at a depth of 1498.5–1498.8 m at *in situ* temperature and pressure: $T = 63\ ^{\circ}C$ and $P = 12.5$ MPa.[21] The Paaratte sandstone in Krevor *et al.*[13] has a porosity of 28.3% and an absolute permeability of 1156 mD, while the Paaratte sandstone in Reynolds[21] has a porosity of 28% and an absolute permeability of 2328 mD. The high absolute permeability values imply that the tested samples may carry many macropores. Through X-ray measurements, Krevor *et al.* [13] found that there were three low-porosity bedding planes perpendicular to the flow direction for the tested Paaratte sandstone core. For comparison purposes, those measures from Krevor *et al.*[13] and Reynolds[21] are plotted and compared with the results in this work (calculated from history matching method) in Fig. 6. The relative permeability curve to water from Krevor *et al.*[13] is smaller than the relative permeability curve for Core 3V over a large range of brine (or water) saturation, but the trend is quite similar. The CO_2 relative permeability from Krevor *et al.*[13] is greater than that of Core 3V, while their endpoint values are quite similar. The similarity in the brine (or water) and CO_2 relative permeability curves suggests that the sandstone from Paaratte formation with relatively large macropores (or high absolute permeability) may have similar behaviors when flooding CO_2 into the formation.

Reynolds performed the core flooding at two different total injection rates, that is 20 and 2 mL min^{-1}, referred to as viscosity-limited and capillarity-limited conditions.[21] The brine relative permeability with an injection rate of 20 mL min^{-1} is similar to that of Kervor *et al.*[13] and those of Core 3V, but the CO_2 relative permeability is slightly lower. When comparing the two injection cases of Reynolds's work, it seems the relative permeability curves moved from low to high brine saturation, with the decrease of the total injection rate. This suggests that the lower irreducible brine saturation can be achieved at a higher injection rate for homogenous Paaratte sandstone, but their relationship also depends on the local

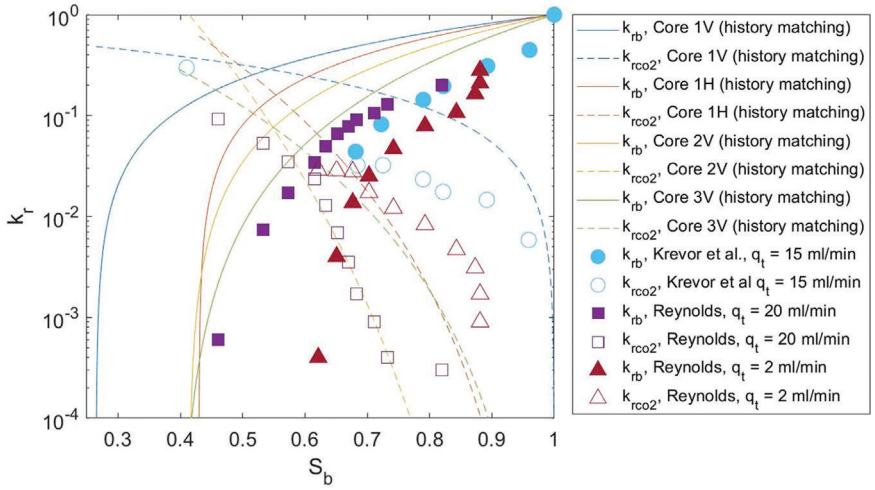

Figure 6. The relative permeability curves at different brine saturation (S_b) for Cores: 1V, 1H, 2V, and 3V, obtained from the history matching method. The relative permeability curves for Paaratte formation at a depth of ~1400 m (Krevor *et al.*[13]) and at a depth of ~ 1500 m are shown for comparison (Reynolds[21]), where q_t in the legend is the total injection rate for both fluids.

heterogeneities in the core.[21] In addition, low CO_2 endpoint relative permeability was observed in both injection scenarios and in Core 3V as well. It was also pointed out and verified by Kervor *et al.*[13] that the low endpoint relative permeability and irreducible brine saturation were limited by the capillary pressure achieved in the experiment and may not reflect the real endpoint values. Those low CO_2 permeability values obtained in Core 3V and in Reynolds[21] may suggest that low CO_2 injectivity can be achieved during the injection in the high permeable region in Paaratte formation.[6]

In this work, the unsteady-state core flooding test was performed, and the one-dimensional core flooding model was carried out to obtain the relative permeability by assuming the core is homogenous. More precise experimental studies are needed to obtain the relative permeability more accurately by considering the rock heterogeneity in the future. Besides, one can utilize X-ray imaging to obtain the local in-situ heterogeneity information of the rock during the experiment, such as capillary heterogeneity. This can help in better understanding how heterogeneity affects multiphase flow and relative permeability behavior in a more general case. Krause *et al.* developed a method to accurately characterize the rock heterogeneity with a 3D core flooding numerical model,[40] and it has been used to study the effect of flow-rate on both effective relative permeability (core-averaged property) and characteristic relative permeability (local property assigned to the voxels in the model).[41] Their results suggest that using a 3D heterogeneous model can generate more accurate estimates of the characteristic relative permeability for heterogenous rock, compared to the one-dimensional homogenous models, given that the 3D model has an accurate permeability distribution as an input. Later, Jackson *et al.* also extended the characterization methods to calibrate the 3D model with multiple fractional flow and multiple flow rate experiments to improve the accuracy of the model.[42] After calibration, the model was applied to obtain the effective relative permeability over a wide range of capillary numbers. The experimental work reported here is limited by the current experimental setups and can only measure the relative permeability for the bulk core. The use of X-ray imaging techniques for measuring the local liquid saturation in the steady-state core flooding experiments can be considered in the future to accurately determine the multiphase flow properties of the heterogenous rock.

Conclusion

Mercury injection capillary pressure tests and nonstationary core flooding tests were performed to measure the capillary pressure, pore size distribution, absolute brine permeability, and relative permeability

of different types of sandstones in the Paaratte formation, at a depth that is relevant to the injection of CO_2 in the CO_2CRC Otway project. Different pore size distributions and absolute permeability were observed from the three types of rock at near-reservoir conditions. The average pore size has been found to vary from 1.93 to 45.8 μm, and the absolute permeability varies between 0.11 and 330 mD. There is a positive correlation between the median pore diameter (and average pore diameter) and absolute permeability. The JBN method cannot obtain the relative permeability curves for CO_2 and brine accurately due to its simplifications and assumptions. The sandstone with a large fraction of macropores (with an average pore size of 45.8 μm) follows a trend of brine relative permeability curve similar to those reported in the literature.[13,21] However, the brine relative permeability of the sandstone with a large fraction of micropores (with an average pore size of 1.93 μm) is higher than that of the highly permeable Paaratte sandstones (permeability $>$ 1 Darcy) reported in the literature.[13,21] In addition, relatively low endpoint values of the CO_2 relative permeability are observed for Core 3V and the Paaratte sandstone reported in the literature,[13,21] and these values may dominate the CO_2 flow during and after the injection. However, relatively large endpoint permeability values are found in Cores 1V, 1H, and 2V, and there is no correlation between the endpoint permeability values and the average pore sizes of the tested samples. The new relative permeability data for the Paaratte formation, specifically, for the distal mouthbar and proximal mouthbar facies in the Paaratte formation, can be used in reservoir simulations to evaluate and predict the pressure buildup in the reservoir and the movement of CO_2 plume during and after injections, as well as CO_2 storage capacity.

Acknowledgments

This work was supported in part by the Australian Research Council through Discovery Projects (DP170102886 and DP190102954). We acknowledge the CO_2CRC Otway Project for providing the sandstone samples for analysis. This research was undertaken and supported with the assistance of resources and services from the National Computational Infrastructure (NCI), which is supported by the Australian Government, and the University of Sydney's HPC service at The University of Sydney.

References

1. Lokhorst A and Wildenborg T, Introduction on CO_2 Geological storage-classification of storage options. *Oil Gas Sci Technol* **60**(3):513–5 (2005).
2. Underschultz J, Boreham C, Dance T, Stalker L, Freifeld B, Kirste D *et al.*, CO_2 storage in a depleted gas field: An overview of the CO2CRC Otway Project and initial results. *Int J Greenhouse Gas Control* **5**(4):922–932 (2011).
3. Watson M, Pevzner R, Dance T, Gurevich B, Ennis-King J, Glubokovskikh S *et al.*, The Otway Stage 2C Project–End to end CO_2 storage in a saline formation, comprising characterisation, injection and monitoring. Paper presented at 14th Greenhouse Gas Control Technologies Conference. 21–25 Oct, Melbourne, Australia. (2018).
4. Dance FM, Geological characterisation of Australia's first carbon dioxide storage site. Dissertation Australian School of Petroleum, University of Adelaide, Adelaide, Australia (2019).
5. Mishra A, Pajank L and Haese RR, High resolution characterization of lithological heterogeneity of the paaratte formation, Otway Basin (Australia), a coastal to shallow-marine deposit. *Geosciences* **9**(6):278 (2019).
6. Mathias SA, Gluyas JG, de Miguel GJGM, Bryant SL and Wilson D, On relative permeability data uncertainty and CO_2 injectivity estimation for brine aquifers. *Int J Greenhouse Gas Control* **12**:200–212 (2013).
7. Oostrom M, White M, Porse S, Krevor S and Mathias S, Comparison of relative permeability–saturation–capillary pressure models for simulation of reservoir CO_2 injection. *Int J Greenhouse Gas Control* **45**:70–85 (2016).
8. Pollyea RM, Influence of relative permeability on injection pressure and plume configuration during CO_2 injections in a mafic reservoir. *Int J Greenhouse Gas Control* **46**:7–17 (2016).
9. Li C, Maggi F, Zhang K, Guo C, Gan Y, El-Zein A *et al.*, Effects of variable injection rate on reservoir responses and implications for CO_2 storage in saline aquifers. *Greenhouse Gases Sci Technol* **9**(4):652–671 (2019).
10. Bennion B and Bachu S, Drainage and imbibition relative permeability relationships for supercritical CO_2/brine and H_2S/brine systems in intergranular sandstone, carbonate, shale, and anhydrite rocks. *SPE Reservoir Eval Eng* **11**(03):487–496 (2008).
11. Bachu S, Drainage and imbibition CO_2/brine relative permeability curves at in situ conditions for sandstone formations in western Canada. *Energy Procedia* **37**:4428–4436 (2013).
12. Pini R and Benson SM, Simultaneous determination of capillary pressure and relative permeability curves from core-flooding experiments with various fluid pairs. *Water Resour Res* **49**(6):3516–3530 (2013).
13. Krevor SC, Pini R, Zuo L, Benson SM, Relative permeability and trapping of CO_2 and water in sandstone rocks at reservoir conditions. *Water Resour Res* **48**(2) (2012). https://doi.org/10.1029/2011WR010859
14. Jeong GS, Lee J, Ki S, Huh D-G and Park C-H, Effects of viscosity ratio, interfacial tension and flow rate on hysteric relative permeability of CO_2/brine systems. *Energy* **133**:62–69 (2017).

15. Tsuji T, Jiang F and Christensen KT, Characterization of immiscible fluid displacement processes with various capillary numbers and viscosity ratios in 3D natural sandstone. *Adv Water Resour* **95**:3–15 (2016).
16. Bachu S, Bennion B, Effects of in-situ conditions on relative permeability characteristics of CO_2-brine systems. *Environ Geol* **54**(8):1707–1722 (2008).
17. Liu N, Ghorpade SV, Harris L, Li L, Grigg RB, Lee RL, The effect of pressure and temperature on brine-CO_2 relative permeability and IFT at reservoir conditions. Paper presented at SPE Eastern Regional Meeting. 13–15 Oct, Morgantown, WV. (2010).
18. Paterson L, Boreham C, Bunch M, Ennis-King J, Freifeld B, Haese R *et al.*, The CO_2CRC Otway stage 2b residual saturation and dissolution test: test concept, implementation and data collected. Milestone Report to ANLEC, CO_2CRC Report No: RPT11-3158 (2011).
19. Dance T, Assessment and geological characterisation of the CO_2CRC Otway Project CO_2 storage demonstration site: From prefeasibility to injection. *Mar Pet Geol* **46**:251–269 (2013).
20. Vidal-Gilbert S, Tenthorey E, Dewhurst D, Ennis-King J, Van Ruth P and Hillis R, Geomechanical analysis of the Naylor Field, Otway Basin, Australia: Implications for CO_2 injection and storage. *Int J Greenhouse Gas Control* **4**(5):827–839 (2010).
21. Reynolds CA, Two-phase flow behaviour and relative permeability between CO_2 and brine in sandstones at the pore and core scales. Ph.D. Thesis, Imperial College London (2016).
22. Al-Quraishi A and Khairy M, Pore pressure versus confining pressure and their effect on oil–water relative permeability curves. *J Pet Sci Eng* **48**(1-2):120–126 (2005).
23. Dance T, LaForce T, Glubokovskikh S, Ennis-King J and Pevzner R, Illuminating the geology: Post-injection reservoir characterisation of the CO_2CRC Otway site. *Int J Greenhouse Gas Control* **86**:146–157 (2019).
24. Johnson E, Bossler D and Bossler V, Calculation of relative permeability from displacement experiments. *Trans AIME* **216**(01):370–372 (1959).
25. Purcell W, Capillary pressures-their measurement using mercury and the calculation of permeability therefrom. *J Pet Technol* **1**(02):39–48 (1949).
26. Georgiadis A, Maitland G, Trusler JM and Bismarck A, Interfacial tension measurements of the (H_2O+ CO_2) system at elevated pressures and temperatures. *J Chem Eng Data* **55**(10):4168–4175 (2010).
27. LaForce T, Ennis-King J, Boreham C and Paterson L, Residual CO_2 saturation estimate using noble gas tracers in a single-well field test: The CO2CRC Otway project. *Int J Greenhouse Gas Control* **26**:9–21 (2014).
28. Lemmon EW, McLinden MO and Friend DG, Thermophysical properties of fluid systems, in *NIST Chemistry WebBook, NIST Standard Reference Database Number 69*, ed. by Linstrom PJ and Mallard WG. National Institute of Standards and Technology, Gaithersburg, MD.
29. Lie K-A, *An introduction to reservoir simulation using MATLAB/GNU Octave: User guide for the MATLAB Reservoir Simulation Toolbox (MRST*) Cambridge University Press, Cambridge, UK (2019).
30. Manasipov R and Jenei B, (eds)., Automated interpretation tool for synchronous history matching of multiple SCAL experiments with advance Nurbs representations of relevant functions. Paper presented at SPE Europec, Virtual. https://doi.org/10.2118/200559-MS
31. Brooks RH and Corey AT, Hydraulic properties of porous media. Hydrology papers (Colorado State University) no. 3 (1964).
32. Meyer K and Klobes P, Comparison between different presentations of pore size distribution in porous materials. *Fresenius' J Anal Chem* **363**(2):174-8 (1999).
33. Yu B-W, Du Y-J, Jin F and Liu C-Y. Multiscale study of sodium sulfate soaking durability of low plastic clay stabilized by reactive magnesia-activated ground granulated blast-furnace slag. *J Mater Civ Eng* **28**(6):04016016 (2016).
34. Bennion DB and Bachu S, editors. The impact of interfacial tension and pore size distribution/capillary pressure character on CO_2 relative permeability at reservoir conditions in CO_2-brine systems. SPE/DOE Symposium on Improved Oil Recovery. *22–26 Apr*, Society of Petroleum Engineers, Tulsa, OK (2006).
35. Shedid SA, Vertical-horizontal permeability correlations using coring data. *Egypt J Pet* **28**(1):97–101 (2019).
36. Bakhshian S, Hosseini SA and Lake LW, CO_2-brine relative permeability and capillary pressure of Tuscaloosa sandstone: Effect of anisotropy. *Adv Water Resour* **135**:103464 (2020).
37. Zhao B, MacMinn CW and Juanes R, Wettability control on multiphase flow in patterned microfluidics. *Proc Natl Acad Sci U S A* **113**(37):10251–10256 (2016).
38. Müller N, Supercritical CO_2-brine relative permeability experiments in reservoir rocks—Literature review and recommendations. *Transp Porous Media* **87**(2):367–383 (2011).
39. Levine JS, Goldberg DS, Lackner KS, Matter JM, Supp MG and Ramakrishnan T, Relative permeability experiments of carbon dioxide displacing brine and their implications for carbon sequestration. *Environ Sci Techol* **48**(1):811–818 (2014).
40. Krause M, Krevor S and Benson SM, A procedure for the accurate determination of sub-core scale permeability distributions with error quantification. *Transp Porous Media* **98**(3):565–588 (2013).
41. Krause MH and Benson SM, Accurate determination of characteristic relative permeability curves. *Adv Water Resour* **83**:376–388 (2015).
42. Jackson SJ, Agada S, Reynolds CA and Krevor S, Characterizing drainage multiphase flow in heterogeneous sandstones. *Water Resour Res* **54**(4):3139–3161 (2018).

Pengyu Huang

Pengyu Huang received his PhD in Civil Engineering from the University of Sydney in 2019. He is a postdoctoral researcher at the School of Civil Engineering at the University of Sydney in Australia. His research interests include modelling the multiphase interaction at the micro/nano-scales and multi-scale modelling.

Luming Shen

Luming Shen received his PhD in Civil Engineering from the University of Missouri-Columbia, Missouri in 2004. He is a Professor in the School of Civil Engineering at the University of Sydney in Australia. His research interests include multiscale modeling and simulation, mechanical characterization, fluid–solid interaction and multiphase flow.

Yixiang Gan

Yixiang Gan received the Dr.-Ing degree (with summa cum laude) in Mechanical Engineering from the University of Karlsruhe, Germany. He is Associate Professor at School of Civil Engineering at the University of Sydney in Australia and is working on mechanics of heterogeneous media, multi-physics and interface problems.

Yinjie Shen

Yinjie Shen is a Master student in Power Engineering at Qingdao University of Science and Technology in China. His research areas focus on rock thermal conductivity and CO_2-enhanced oil recovery in ultra-low permeability rock. He has been involved in and completed several large projects on porous media.

Dongxing Du

Dongxing Du currently works as a full professor at College of Electromechanical Engineering, Qingdao University of Science and Technology (QUST), China. At the same time, he acts as the vice leader of Geo-Energy Research Institute of QUST. Dongxing Du focuses on and has expertise in the research area of Condensed Matter Physics, Fluid Dynamics, Heat & Mass Transfer, and Thermodynamics in relationship with the Enhanced Oil Recovery and CCUS industry. He has published more than 30 SCI papers and led more than 10 scientific and industrial projects.

Bowei Yu

Dr. Bowei Yu is an expert in specialist testing, research & development in the geotechnical engineering field. He has a PhD degree in geotechnical engineering and has an excellent track of records in research of unsaturated soil mechanics, soil stabilization, contaminated land remediation, and clay liner systems, etc. Dr. Yu is now working as a key member in the specialist testing department in Alliance Geotechnical (Australia), in charge of the running and developing in the advanced soil testing, especially in areas of triaxial, unsaturated, and toxic-related tests.

Federico Maggi

Federico Maggi is Associate Professor in Environmental Engineering and Head of the Environmental Laboratory at The University of Sydney. He is also Guest Faculty Affiliate with the EES at Lawrence Berkeley National Laboratory, CA, USA. He holds a PhD from TUDelft and a ME from Polytechnic University of Torino. His research focuses on environmental modeling of geophysical flows of water, dispersion of chemicals, and bio-physical processes.

Abbas El-Zein

Abbas El-Zein is Professor of Environmental Engineering at the University of Sydney in Australia. He runs the GeoEnvironmental Laboratory at the School of Civil Engineering and is working on problems in unsaturated soil hydrology and soil mechanics, groundwater contamination, computational modeling and environmental risk.

